

Simulated low-frequency modes of circulation in the Arctic Ocean

Sirpa Häkkinen

NASA Goddard Space Flight Center, Greenbelt, Maryland

Cathleen A. Geiger¹

Universities Space Research Association, NASA Goddard Space Flight Center, Greenbelt, Maryland

Abstract. The variability of the Arctic circulation is investigated for a 43 year period (1951–1993) from a coupled ice-ocean model. Empirical orthogonal function (EOF) analysis shows that the variability of the sea surface height (SSH) and vertically integrated transport is organized so that in the leading mode the whole Arctic operates as a single gyre. The mode is associated with the Arctic Oscillation (AO) [Thompson and Wallace, 1998], and it explains over 70% of the variance in the vertically integrated transport and 25% of the SSH variability. The physical interpretation of this mode is derived to arise from its close connection to the Atlantic inflow to the Arctic. The mode shows a major shift toward cyclonic circulation in the end of the 1980s which is associated with a large multiyear pulse of Atlantic water to the Arctic. Thus this event appears as the likely initiation of the Atlantic layer warming observed during the recent years [Carmack *et al.*, 1995]. Overall, the first mode shows strong decadal variability as reported by Proshutinsky and Johnson [1997]. The second mode of the oceanic circulation, which explains 9% of the variance in the transport, contains two gyres with opposing cyclonicity in the Eurasia and Canada basins. It projects onto the North Atlantic Oscillation (NAO) pattern and displays a 14 year cycle which is known to exist in the midlatitude North Atlantic surface temperatures [Deser and Blackmon, 1993]. A further examination reveals that this mode describes the variability of the flow through the Barents Sea, which is modulated by the water mass modification due to the local heat flux variability. The apparent NAO connection is provided by a simultaneous correlation between the time series of this second mode and the leading heat flux mode in the North Atlantic which is associated with NAO.

1. Background

The variability of sea ice has long been considered an indicator of climate changes, and with increasing and improving databases for polar regions, the Arctic climate is receiving wider attention. Of particular interest is the search for possible anthropogenic changes against a background of natural variability of the global atmosphere-ocean and ice system. One of the few continuous data sets with extensive coverage for studying ice-related processes are the satellite passive microwave observations which are available since November 1978. This data set was used in a recent study of Cavalieri *et al.* [1997] which showed a declining trend in sea ice extent in the north polar regions for the last 18 years. Since the time series is still short with respect to climate variability, it is not known if the trend is part of a natural long-period variation or associated with anthropogenic global warming. Besides this sea ice trend, the recent decade (1980s) in the Arctic has seen large-scale changes in atmospheric circulation, the oceanic circulation, and associated water mass properties: The sea level pressures

over the Arctic have decreased dramatically, signifying an anomalous cyclonic circulation of the atmosphere [Walsh *et al.*, 1996]. At the same time the Atlantic layer in the Arctic at 200–500 m depth has been warming by $\sim 1.5^{\circ}\text{C}$ [Carmack *et al.*, 1995]. The warming of the Atlantic layer is associated with a westward frontal shift of eastern and western type halocline waters from the Lomonosov Ridge to the Alpha and Mendeleev Ridges [Carmack *et al.*, 1995; MacLaughlin *et al.*, 1996]. It is likely that these two phenomena are linked together because enhanced cyclonicity of the atmospheric circulation would favor cyclonic spreading of water masses and reduced ice cover in the Greenland Sea and eastern parts of the Arctic Ocean.

The last two decades are also characterized by unusual strength of the North Atlantic Oscillation (NAO) [Hurrell, 1995], which has reached a very high positive index. For a positive NAO phase the Icelandic low is stronger than usual, while in the Greenland Sea the northerly winds are weaker than usual. NAO also has a southern center near the Azores which has a high-pressure anomaly at the positive index phase of NAO. Besides the association with distinct pressure anomalies, NAO reflects the variability of the storm tracks in the North Atlantic with more storms tracking the NE route from Labrador to the Norwegian Sea and farther toward the Barents Sea at the positive index phase [Serreze *et al.*, 1997]. During the negative NAO index the storms are less frequent and more aligned along 45°N latitude line. Changes in the Arctic synoptic

¹Now at Department of Geography, University of Delaware, Newark.

activity have also occurred with an increase in storm frequency since 1950s to 1980s [Serreze *et al.*, 1993]. The notion that the Arctic atmospheric variability can be closely related to the midlatitude patterns was brought up in the rotated empirical orthogonal function (EOF) analysis of 500 hPa heights by Cheng *et al.* [1995]. Their analysis shows that the Arctic is covered by the same NAO-like pattern that extends to the midlatitudes of the North Atlantic. NAO in sea level pressures (SLP) appears as a leading mode if EOF analysis of SLP is limited to the North Atlantic sector, but EOF analysis of the whole Northern Hemisphere SLP produces a pattern centered in the Arctic. The pattern resembles NAO, but recently, Thompson and Wallace [1998] have proposed that this pattern reflects the strength of the polar vortex above and suggested a name "Arctic Oscillation" (AO). This anomaly pattern has a rather symmetric low SLP center over the central Arctic with a southward extension of low SLP in the Greenland Sea sector and a high SLP center at $\sim 40^\circ\text{N}$ both in the North Atlantic and North Pacific. This pressure pattern is similar to the SLP pattern associated with the seesaw between Greenland and Scandinavian winter air temperatures identified by van Loon and Rogers [1978]. The close relation between NAO and AO is emphasized by the high correlation between the NAO index and AO time series [Thompson and Wallace, 1998].

The signatures of NAO in sea ice have been explored in a study by Agnew [1993], who showed that a pressure composite corresponding to heavy ice condition years minus light ice condition years over the whole Arctic resembles the NAO pattern in its negative phase. Fang and Wallace [1994] investigated sea ice conditions and 500 hPa variability at lag/leads from weeks to years and found the strongest relationship for 500 hPa leading sea ice by 2 weeks. They also show that the most dominant variability in ice conditions, the seesaw between Davis Strait/Labrador Sea and Greenland/Barents Seas ice conditions, is related to NAO. The timescales associated with NAO cover the whole spectrum from very high frequency (a few days) to lower frequencies, such as quasi-biennial (2–3 years) and subdecadal periods (~ 8 years) [van Loon and Rogers, 1978]. The subdecadal NAO oscillation signature has been identified in the geochemistry of the Greenland Ice Sheet cores [Barlow *et al.*, 1993] and attributed to the decadal-scale temperature variations in the northwest Atlantic as inferred from Labrador tree rings [D'Arrigo *et al.*, 1996]. While SLP itself does not display a significant 12–14 year periodicity, analyses of midlatitude joint modes with surface temperature often produce significant peaks at quasi-decadal (10–14 years) periods. The midlatitude North Atlantic surface temperatures associated with NAO displays a distinct variability at 12–14 year periods [Deser and Blackmon, 1993]. In the Arctic, a decadal cyclicity is found by Proshutinsky and Johnson [1997], who describe the ice drift and barotropic ocean current system as having 5–7 year regimes of anticyclonic and cyclonic rotation resulting from fluctuations of the strength between Icelandic low and Siberian high.

The objective of this study is to investigate this extraordinary variability by using a stratified ocean model coupled to a fully dynamic-thermodynamic ice model. We apply principal component analysis to explore spatial and temporal variability in the high northern latitudes and thus offer a complementary perspective to the study by Proshutinsky and Johnson [1997]. Our study is a hindcast from 1946 to 1993 using Comprehensive Ocean and Atmosphere Data Set (COADS) anomalies [daSilva *et al.*, 1994] added to a monthly climatology compiled

from different sources. In the Arctic the monthly wind speed and wind stress climatology is constructed from NCAR $5^\circ \times 5^\circ$ SLP data set (1946–1993). The interannual forcing is thus provided directly by geostrophic wind stress and wind speed computed from the same SLP data set. Analysis is done for the period 1951–1993. The coupled ice-ocean model used in this study has been previously described in studies by Mellor and Kantha [1989] and Häkkinen and Mellor [1992]. The 10 year quasi-equilibrium run from which the 48 year simulation starts is presented by Mauritzen and Häkkinen [1997]. The ice and ocean models and their initialization are briefly summarized in section 2. The model results are presented in section 3: First, in section 3.1, atmospheric modes of variability are discussed. Anomalous ice drift and ice export are explored in section 3.2. The Arctic Ocean circulation and Atlantic water inflow to the Arctic are presented in sections 3.3 and 3.4.

2. Coupled Model

2.1. Model Description and Model Grid

The ocean model is hydrostatic and Boussinesq and uses the σ coordinate system as described by Blumberg and Mellor [1987] with a modified scalar advection scheme to avoid overshooting at sharp fronts [Mauritzen and Häkkinen, 1997]. The 2.5-level turbulence closure scheme of Mellor and Yamada [1982] is used to determine the vertical mixing coefficients for momentum and scalar variables. The dynamic-thermodynamic ice model is coupled to the ocean model via interfacial stresses and via salinity and heat fluxes through the ice-water interface. The ice model uses a generalized viscous rheology as discussed by Häkkinen and Mellor [1992].

The coupled ice-ocean model extends from the Bering Strait to 15°S with resolution of 7/10 in "longitude," 9/10 in "latitude" (in a rotated coordinate system with equator at 30°W and the pole at 120°W , 0°N). There are a total of 20 σ -levels in the vertical with higher resolution near the surface. To minimize the inaccuracies in the computation of the pressure gradient, the topography (derived from the TerrainBase Global DTM database with $5' \times 5'$ resolution) is smoothed heavily, but simultaneously with the smoothing, the important passages and sills are restored to near their original depth. Also, the major islands and two passages through the Canadian Archipelago are retained.

2.2. Initialization and Forcing of the Coupled Model

The initialization of this simulation is taken from the end of the tenth simulation year of a quasi-equilibrium run presented by Mauritzen and Häkkinen [1997], where the average ice export from the Arctic is tuned to be 2000 km^3 per year. By the tenth year the Rossby adjustment has taken place while the deep ocean evolves slowly. The quasi-equilibrium run was initialized with the annual average hydrographic climatology of Levitus *et al.* [1994] and Levitus and Boyer [1994]. The transports at oceanic lateral boundaries were specified to be 0.8 Sv through the Bering Strait and 0.8 Sv out at 15°S . At the southern boundary the salinities and temperatures are relaxed to Levitus values in five grid rows from the boundary. Immediate restoring of temperature T and salinity S is used at the Mediterranean outflow point.

The 10 year initialization run is forced with monthly climatological data. The surface stress climatology is a combination of the Trenberth *et al.* [1989] monthly European Centre for Medium-Range Weather Forecasts (ECMWF) wind stress cli-

matology over open ocean and of a geostrophic wind stress (derived from National Center for Atmospheric Research (NCAR) 5×5 surface pressure and averaged over 1946–1993) over sea ice with an exchange coefficient of 1.3×10^{-3} , which are blended to each other at the boundary to avoid unphysical vorticity source. For the heat exchange the bulk formulation is adopted where the heat fluxes are a function of the oceanic surface quantities. The heat exchange with coefficient of 1.3×10^{-3} is used regardless of air-ocean stability conditions. The surface humidity is computed from model-generated surface temperature with 98% saturation. The other base climatological fields, air temperature, humidity, and wind speed, are from ECMWF climatology. Short-wave and downward long-wave radiation require cloudiness information which is given by International Satellite Cloud Climatology Project (ISCCP) measurements. The precipitation minus evaporation ($P-E$) field is obtained from National Centers for Environmental Protection (NCEP) operational analysis [Rasmusson and Mo, 1996] averaged for 5 years. When the river runoff (a combination of sources from Pocklington [1987] and Russell and Miller [1990]) with an annual total of $18,000 \text{ km}^3$ is included, modifications were added to the $P-E$ field at 8° – 12°N to conserve salt in the basin.

After the 10 year spin-up, COADS anomalies from 1946 to 1993 (air temperature, mixing ratio of the air, wind stress, and wind speed) [daSilva et al., 1994] are added to the above described climatology everywhere south of 60°N . To include interannually varying wind-driven forcing in the high latitudes, the wind stress and wind speed were given somewhat different treatment as the COADS does not contain adequate data north of 60°N . At high latitudes we compute geostrophic wind stress and wind speed from NCAR 5×5 SLP data, which were the basis for the climatology. COADS wind anomalies transition to geostrophic wind anomalies by linear blending in the region, 50° – 60°N (geostrophic winds are interpolated to the COADS $1^\circ \times 1^\circ$ grid first). Everywhere in the model, region cloudiness, precipitation minus evaporation field, and river runoff continue to be climatological.

The choice of COADS anomalies and the above climatology was preferred because the model itself is geared for the whole Arctic–North Atlantic system even though NCEP/NCAR Reanalysis became available in 1997. Considering the whole basin, the climatology used gives rather a stable and realistic oceanic climatology without significant drifts in temperature and salinity fields. On the other hand, COADS provides an extensive time series of observational anomaly fields for atmospheric surface quantities and oceanic quantities in creating heat-flux anomalies.

3. Results

The goal of this study is to seek relationships between ice, ocean, and atmospheric circulation. The analysis of the ice and ocean motion covers 1951–1993, neglecting the first 5 years, i.e., 1946–1950, during which the midlatitude Rossby waves have crossed the Atlantic at least once. The Arctic ocean spin-up is expected to be rapid owing to weak stratification, but considering the lower latitude influence where the oceanic adjustment is slower, we neglect the first 5 years. It is recognized that the dynamic spin-up of the Arctic ice motion takes place within 1 day, but thermodynamic spin-up of the ice system is much slower. However, we expect the ice mass balance is not far (within 20%) from the 10 year climatology used to

initialize the simulation at year 1946. Another reason to concentrate only on the dynamic quantities is that the surface forcing in the Arctic does not have interannually varying cloudiness and air temperatures. The neglect of interannually varying thermodynamics is unlikely to influence the primary modes of ocean circulation because their dynamics are either driven by wind stress or heat flux in the open water. The approximation of using climatological air temperatures and humidities in the open water heat flux at high latitudes is unlikely to be a significant problem at low frequencies at which Halliwell and Mayer [1996] show that wind speed anomalies are more important than air temperature anomalies.

3.1. Leading Modes of Atmospheric Circulation

To date, the NCAR SLP fields are the best documented data set for the Arctic and are used in this model simulation for derivation of the wind stress fields over the Arctic. We apply an EOF analysis on the SLP anomaly (SLPA) fields (1946–1995) to give a suitable reduction in information of the main atmospheric circulation features for comparison with ice and ocean circulation regimes. The first SLP EOF mode explaining 19% of the variance is shown in Figure 1a and has been called Arctic Oscillation by Thompson and Wallace [1998]. The spatial pattern consists of a large, elongated low-pressure anomaly extending from the central Arctic to the Greenland Sea with high-pressure anomalies near Azores and Aleutian Islands. The second SLP mode (Figure 1b) accounts for 10% of the variance and appears to be a mixture of NAO and Pacific–North American (PNA) teleconnection patterns, with a negative phase NAO signature of a high-pressure center over Greenland straddling the Canada Basin and a low-pressure center near Azores. PNA association comes from the strong high-pressure anomaly at the Aleutian Islands. In mode 1, Icelandic low-pressure anomalies are inversely related to Aleutian low-pressure anomalies, but in mode 2 the two low-pressure centers are in phase. The mode 1 SLPA pattern is similar to the SLPA pattern associated with the seesaw between Greenland and Scandinavian winter air temperatures identified by van Loon and Rogers [1978]. Mode 2 resembles another SLPA pattern described by van Loon and Rogers [1978], where both Greenland and Scandinavia air temperatures are above (or below) the long-term mean.

The first principal component (PC) of the SLP field (Figure 2) for all months shows less of a trend than the AO defined only on the basis of winter months (November–April) by Thompson and Wallace [1998]. The main significant feature in SLP PC 1 is the shift in the end of 1980s to a cyclonic circulation anomaly. In the central Arctic the pressure decrease was as much as 4 mbar since early 1980s, as reported by Walsh et al. [1996] and Thompson and Wallace [1998]. Besides the spatial pattern, the close association with the NAO index and SLP PC 1 is suggested by a correlation of 0.72 using winter (November–April) values only [Thompson and Wallace, 1998]. A quasi-biennial oscillation is evident in the time series, which was already noted by van Loon and Rogers [1978] as the dominant frequency of the seesaw oscillation where Icelandic and Aleutian low-pressure anomalies are out of phase. Overall, SLP PC 1 has an appearance of white noise; however, from the low-frequency behavior of PC 1 one can pick multiyear periods of strong anticyclonicity around 1960, 1969–1970, 1977–1980, and 1986. The cyclonic periods are centered at 1954, 1964, 1974–1976, 1984, and 1990. The timing of these regimes gives an appearance of an 8–9 year cycle. The power at the 8–9 year

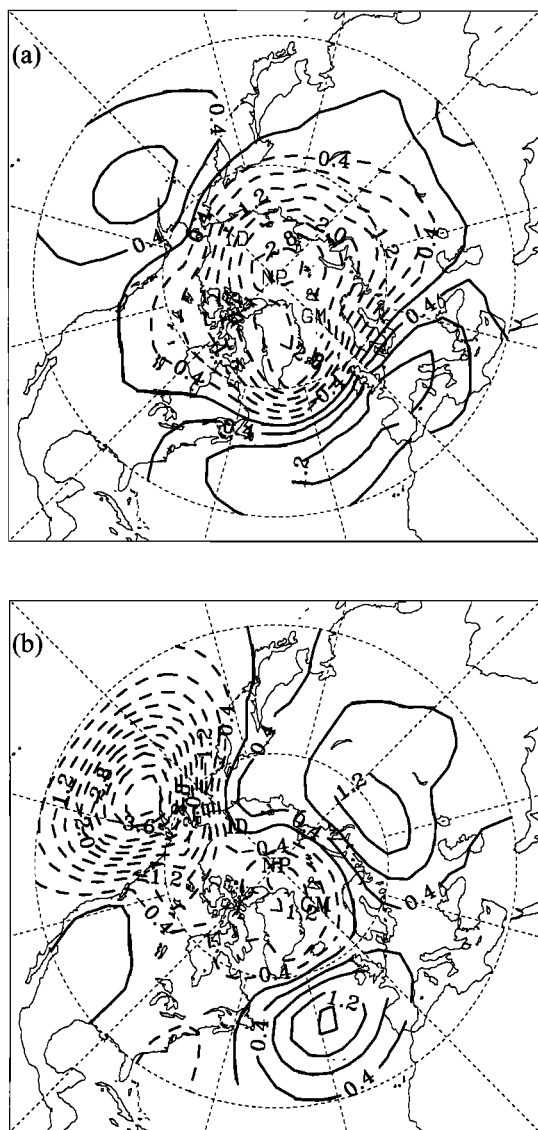


Figure 1. The spatial patterns of the first two empirical orthogonal function (EOF) modes for the sea level pressure. Contour interval is 0.4 hPa.

frequency band in the atmosphere is found to exist through the historic times as manifested in tree rings [D'Arrigo *et al.*, 1996] and in Greenland ice cores [Barlow *et al.*, 1993]. Even though a part of the EOF 2 pattern suggests a relation to NAO, no significant correlations arise between the SLP PC 2 (not shown) and NAO index (from NCEP standard indices). SLP PC 2 (not shown) has no distinguishing features, but it has a strong quasi-biennial oscillation and is highly correlated with the NCEP standardized PNA index, 0.83 between their averaged November–April values.

3.2. Sea Ice Motion and the Leading Modes of Circulation in the Atmosphere

Since the sea ice is mainly wind-driven, we expect the ice motion to exhibit similar patterns as the SLP field. The simulated 43 year average ice motion is shown first in Figures 3a and 3b, displaying the well-known anticyclonic pattern (the field shows that the area around Iceland contains on average too much ice). To highlight the variability superimposed on

this pattern as forced by the leading atmospheric circulation mode, we will construct a composite of anomalous ice motion. Composite differences for ice drift are computed at the extrema of the SLP PC 1 (AO) exceeding one standard deviation by subtracting ice drift fields corresponding to negative extrema from the fields corresponding to positive extrema. All months are included in the composites, and no detrending has been applied to the fields. These composites and areas where the differences are significant at 95% level are shown in Figures 4a and 4b. As anticipated, the ice motion following the geostrophic winds associated with the SLP EOF 1 gives a pattern where ice motion is cyclonic around the periphery, which results in northward ice drift in the Kara-Barents-Greenland Seas and southward ice drift in Baffin Bay (Figure 4a). The latter gives rise to the well-known seesaw in the ice extent between the European sector (Kara-Barents Seas) and Baffin Bay. The SLP EOF 1/AO does not enhance the Transpolar Drift Stream transport of sea ice because the Drift Stream is located approximately at the ridge of this SLP pattern and is seen from the lack of significant vector differences in Figure 4a. The AO has a strong influence in the western Arctic where, depending on the phase of the AO, the sea ice buildup would occur in the Laptev and East Siberian Seas (negative AO) or in the Beaufort Sea (positive AO). On the basis of the composite during late 1980s and early 1990s, when AO was strongly positive, the Siberian coast should have had considerably lighter ice cover, which has been confirmed by satellite observations [Parkinson *et al.*, 1998; Serreze *et al.*, 1995]. The SLP EOF 2 pattern (Figure 1b) has a geostrophic wind field associated with it that would appear to force ice out from a large area of the Arctic through the Fram Strait. However, an ice motion composite corresponding to SLP PC 2 fails to show such a relationship; instead, the Arctic main basin ice flows out between Svalbard and Severnya Zemlya (not shown).

From the oceanic point of view the transport of ice out the Arctic to the Greenland-Iceland-Norwegian (GIN) Seas and then farther to the subpolar gyre are of importance for the stratification and renewal of water masses in those two areas and thus for the thermohaline circulation in the North Atlantic [Mauritzen and Häkkinen, 1997]. In the climatological simula-

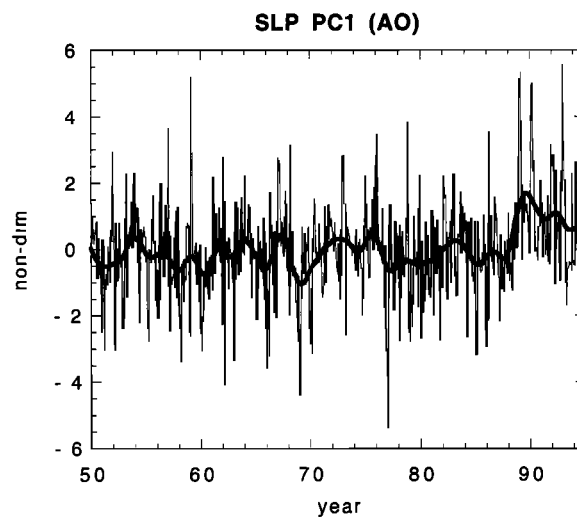


Figure 2. The first sea level pressure (SLP) principal component (PC) shown in nondimensional units (thin line) and low-pass filtered (37 month Hanning) form (thick line).

tion (which is used as the initialization for this run) the annual Fram Strait export is $\sim 2000 \text{ km}^3$. The annual average export for 1946–1993 and for 1951–1993 in the hindcast run are 2015 and 2070 km^3 , respectively, which are very close to the climatological run value and were expected because the climatology was produced from monthly averages over the period 1946–1993. The stability of the export values shows that ice export is determined by linear wind-driven dynamics. The time series of the interannually varying ice export through Fram Strait is shown in Figure 5 together with ice export from the simulation of Häkkinen [1993, 1995], both as annual averages. The fine resolution model [Häkkinen, 1993] gives a maximum ice export in 1968 which is 1800 km^3 above the simulation average. Figure 5 shows that the ice export is rather dependent on the resolution of the model, as both of the models use nearly the same atmospheric forcing: In the present simulation the maximum occurs in 1962, which is 700 km^3 more than the 1968 ice export.

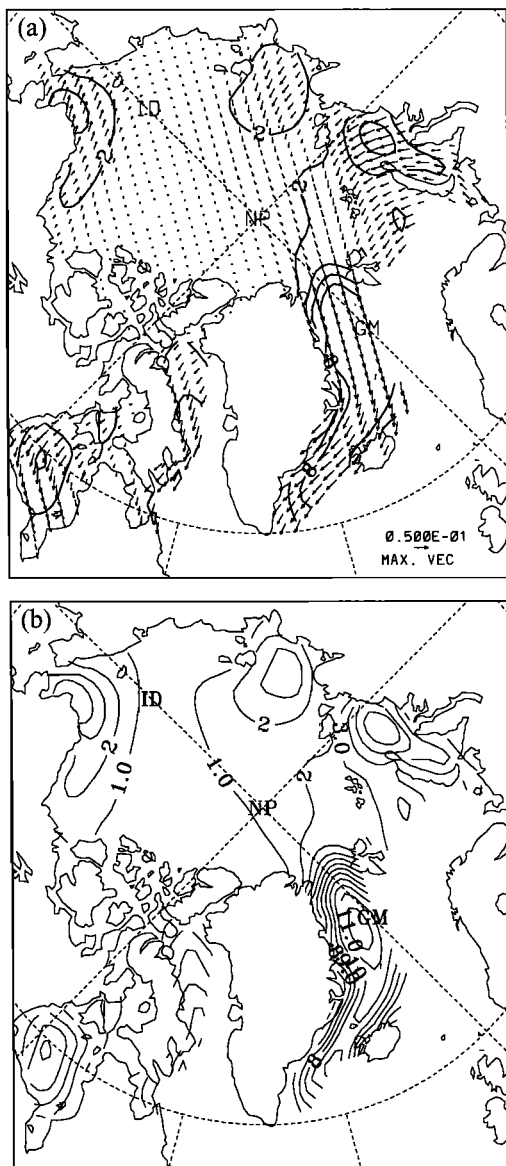


Figure 3. Average ice motion during the 43 year simulation. (a) Ice drift vectors truncated so that maximum velocity is 5 cm/s. Drift speed contours are overlaid with contour interval of 2 cm/s. (b) Average ice drift contours with 1 cm/s interval.

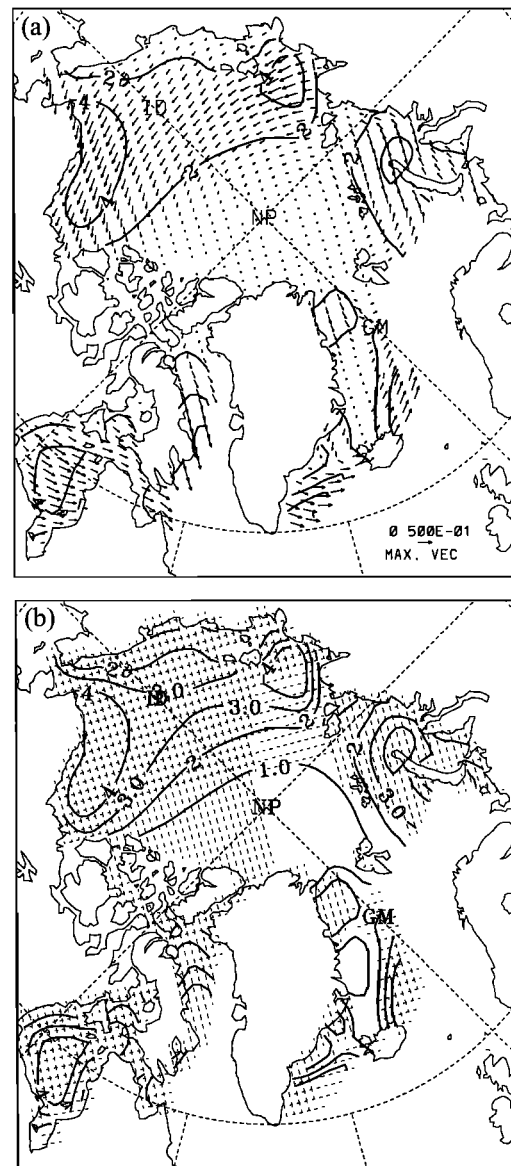


Figure 4. Ice drift composite difference, the monthly maxima (>1 s.d.) of SLP PC 1 minus the minima (<-1 s.d.) of SLP PC 1, all months included to the composite. (a) Vector difference overlaid by drift contour of 2 cm/s, maximum vectors truncated to 5 cm/s. (b) Contours (interval of 1 cm/s) of the absolute value of the vector difference with hatched areas implying that the vector component difference is significant at 95% level. Near-horizontal dashed lines refer to u component, and near-vertical lines refer to v component (dashed lines follow the axii of the grid).

In fact, the coarse resolution simulation of Walsh *et al.* [1985] shows also year 1962 as having the largest ice export in the 1960s. Both of the simulations agree rather well on the timing of the minima and maxima. Overall, the Fram Strait ice export shows a decreased ice export averaging ~ 1600 – 1700 km^3 for the last 10 years. In fact, the average anomalous SLP gradient for the last 10 years of the run gives a weak northward geostrophic stress in agreement with the decreased export. While the Fram Strait export varies by a factor of 3, the Denmark Strait ice export, shown also in Figure 5, is even more variable by a factor as large as 10 or more. It does not appear to have

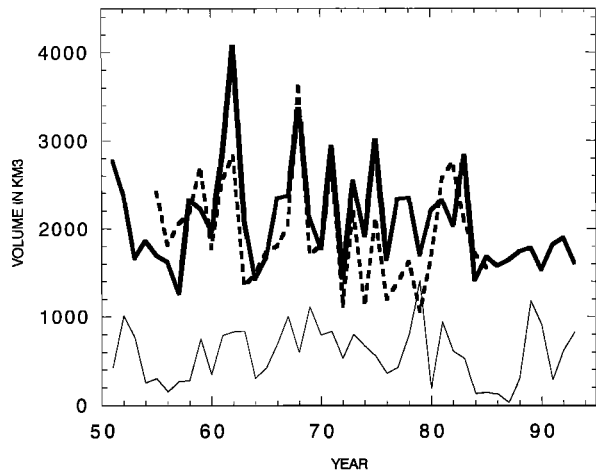


Figure 5. Annual ice export (in km^3): thick solid line, Fram Strait export, this simulation; dashed line, Häkkinen [1995]; and thin solid line, Denmark Strait ice flow, this simulation.

long-term trend like in the Fram Strait export in the simulations, which suggests that they are driven by different atmospheric conditions. One would expect that if the Fram Strait export is large, the Denmark Strait export would increase also, as the Arctic is the main source of sea ice in the GIN Seas. On the contrary, it appears that the Denmark Strait export is often out of phase with the Fram Strait export. This suggests that local atmospheric circulation around Iceland is responsible for the difference in variability for the two Straits.

To explore the atmospheric conditions responsible for the largest monthly export events, a composite of SLPA is constructed from ice export extrema above one standard deviation, so that a SLP field corresponding to negative extrema is subtracted from a SLP field corresponding to positive extrema (months November to April are included in the composite, and detrending is not applied to emphasize the most favorable SLPA fields for ice outflow). The two composites for the ice export at Fram Strait and Denmark Strait are displayed in Figures 6a and 6b. The SLPA pattern for the Fram Strait export (Figure 6a) shares some features with the NAO pressure anomaly pattern at a low index phase, where high-pressure anomaly over Greenland imposes a wind field-enhancing ice drift in the Transpolar Drift Stream, but in addition, it has a strong low-pressure center in the Kara-Barents Seas area. A similar SLPA pattern resulting from regression with ice export has been derived by Hilmer *et al.* [1998]. The sequence of the SLP fields during the Great Salinity Anomaly (GSA) period (1968–1972 [Dickson *et al.*, 1988]) as given by Häkkinen [1993] showed that the largest ice export occurred when there was a secondary low in the Barents Sea. In that model the ice export from the Arctic was well above average for all other seasons except summer during the year of the GSA.

In the work of Häkkinen [1999a] it is shown that for an occurrence of a GSA a large export from the Arctic is prerequisite, but another necessary condition is that the ice export anomalies at the Denmark Strait are significant enough to interrupt the deep convection downstream. Thus a GSA needs a favorable atmospheric circulation local to GIN Seas to push the excess ice through the Denmark Strait to the subpolar gyre. The SLPA pattern for extrema in the Denmark Strait export (Figure 6b) has a strong low-pressure center over Scandinavia

with isobars aligned so that the cyclonic circulation pushes ice into the subpolar gyre. However, this pattern is not a classified teleconnection pattern if Barnston and Livezey [1987] classification is used. This lack of relationship between ice cover around Iceland and leading atmospheric SLP modes was noted by Walsh and Sater [1981]. Rogers [1997] discusses the storm track variability in the North Atlantic and finds that a pattern similar to Figure 6b corresponds to a SLP difference between winters with extremely active cyclone frequency (Icelandic low is very intense and extends to the Norwegian Sea) and winters with a very low frequency of storms.

While the composite pressure pattern corresponding to extrema in the Fram Strait ice export gives a SLPA pattern having some similarity to NAO, a simultaneous strong correlation between the winter averages of the Fram Strait ice ex-

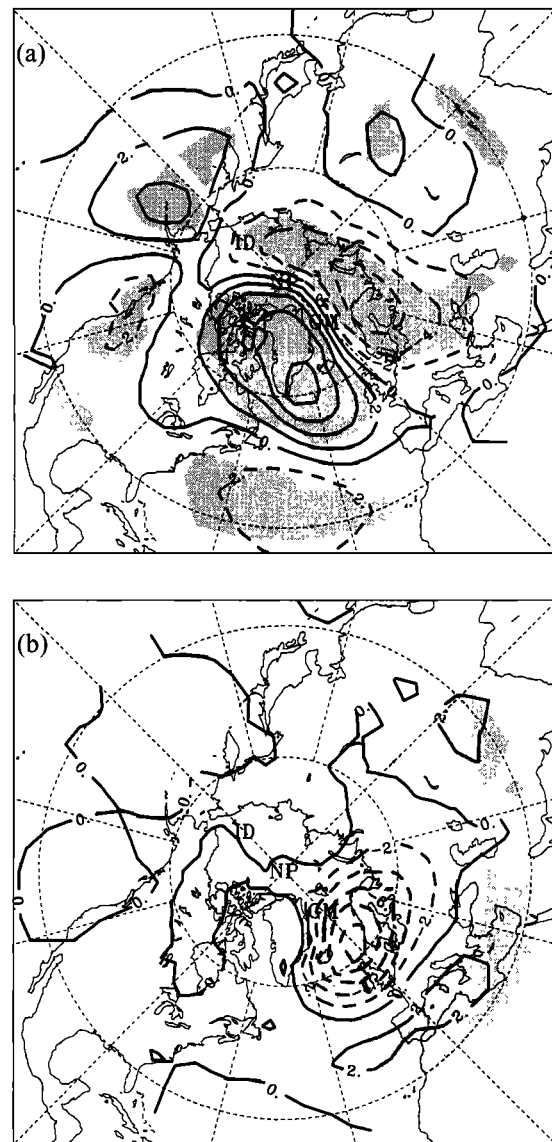


Figure 6. SLP composites for monthly extrema (months November through April) in the (a) Fram Strait and (b) Denmark Strait sea ice exports when they are above one standard deviation. Untrended data for all months is used. Contour interval is 1 hPa. Shading indicates that the difference is significant at 95% confidence level.

port and NAO index fails to materialize. This is not surprising because the NAO index itself mainly measures the strength of the midlatitude westerlies not the properties of the SLP field at the very high latitudes. However, as the SLP composite (Figure 6a) suggests, the large ice export pulses out of the Arctic occur if the prevailing SLPA field is similar to pressure anomalies at the negative phase of NAO. Figure 5 shows that the large exports took place in the 1960s and in the early 1980s when NAO was in a negative phase, and likelihood is high that a SLPA pattern of Figure 6a may also occur. As the ice velocity composites (Figures 4a and 4b) suggest, no significant simultaneous correlations exist between Fram Strait export and SLP PC 1 (nor with SLP PC 2).

3.3. Leading Modes of Circulation in the Arctic Ocean

As the overall stratification in the Arctic is weak, i.e., the high-latitude baroclinic Rossby radius of deformation, $\sim 3\text{--}5$ km, is vanishingly small compared to the midlatitude deformation radius, 50–100 km, the wind driven barotropic circulation should dominate the vertically integrated oceanic transport field and sea surface height (SSH). The 43 year average horizontal stream function, i.e., the vertically integrated transport, for the Arctic (Figure 7a) shows a cyclonic double gyre with maximum transport of 8 Sv in the Eurasia basin and a very weak anticyclonic gyre (-1 Sv) in the Canada Basin. Greenland Sea has a strong cyclonic gyre of its own, also evident in the average SSH (Figure 7b). To study the interannual and longer timescale variability, the EOFs of the monthly stream function and SSH anomalies are computed and are shown in Figure 8. The first oceanic circulation mode contains a monopole of an anomalous circulation which involves the whole Arctic basin, but it also has a large amplitude in the GIN Seas. The vorticity field corresponding to the spatial pattern of the SLP EOF 1 (Figure 1a) gives rotation around the elongated low-pressure anomaly and leads to a transport pattern where the ocean operates in unison like in the stream function EOF 1 (Figure 8a). The second mode reflects the variability of the individual gyres with opposite rotation in the Canada and Eurasia-GIN basins (Figure 8b). The variability of the stream function is highly concentrated in the first EOF mode, which explains 71.6% of the total variance, while the second mode contains 9.2% of the variance. The third mode (not shown) contains 8.1% of the variance and describes opposite sign gyres in the Arctic and GIN Seas; the variance of the mode diminishes below 4% if detrended stream function data are used. The spectral behavior of PC 3 represents merely white noise and is not discussed further.

The first mode of the Arctic SSH appears also as a monopole involving concurrent changes in SSH around the Arctic (Figure 8c). The second mode (Figure 8d) has two dipoles: one dipole between Canada Basin and East Siberian Sea separated by Lomonosov Ridge from another dipole between the Eurasia-GIN basin and the Barents-Kara Seas. The first two modes explain 25 and 13% of the total variance, respectively. The trend in SSH is spread to several modes, and detrending the SSH first modifies slightly the spatial pattern of EOF 2 (not shown), but the variances of modes 1 and 2 are nearly the same, 24 and 12%, as for the untrended data. The stream function spatial patterns are unambiguous, and we concentrate on them after a few general notes about the variability in the time series of the first two modes. The notable difference in the variance of the first SSH and stream function modes can be explained by the fact that the topography puts more constraints

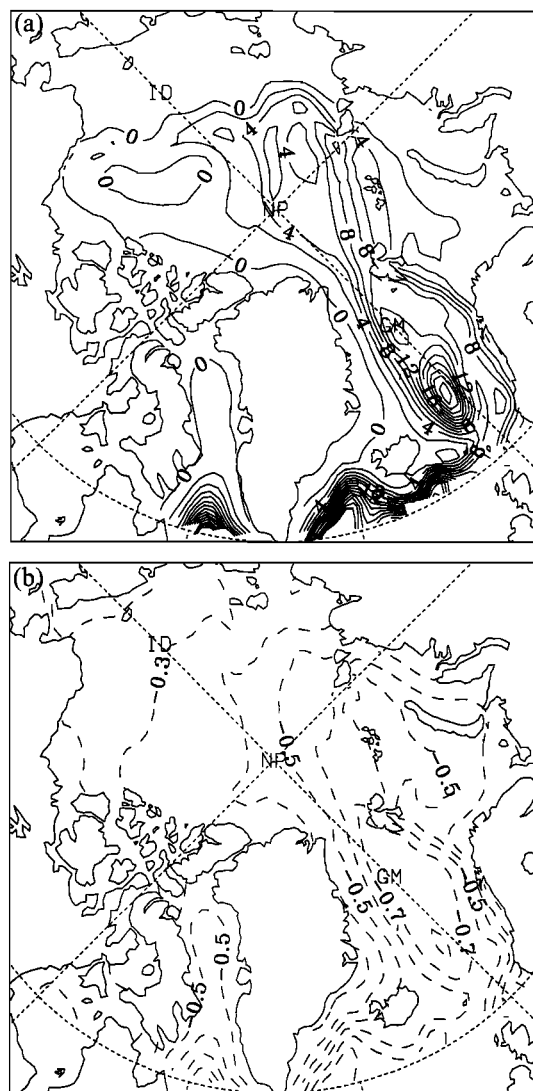


Figure 7. (a) 43 year average oceanic stream function. Contour interval is 2 Sv. Negative values indicate anticyclonic motion, and positive ones indicate cyclonic motion. (b) The 43 year average sea surface height. Contour interval is 0.1 m.

on the stream function than on SSH by greatly diminishing the transport variability across f/h -lines. The very heavily smoothed topography may also concentrate more variance on the first mode of the stream function.

The leading modes of the oceanic stream function and SSH anomalies described by their PC (Figures 9a and 10a in their detrended form) show prominent low-frequency variability; especially the second modes are dominated by quasi-decadal variability. The SSH and stream function PC 1 are highly correlated (0.83) at zero lag, signifying the same driving force. The second modes (Figures 9b and 10b) show somewhat lower frequency variability than the first modes; however, the SSH PC 2 is more irregular than the stream function PC 2. The amplitude of the fluctuations in the stream function PC 1 has increased considerably since mid-1960s. Whether the earlier pressure data were of poor quality or there is a shift in the intensity in the atmosphere-ocean interaction is not known. The trend in the NAO index [Hurrell, 1995] and the increased storminess at high latitudes [Serreze *et al.*, 1997] suggests that

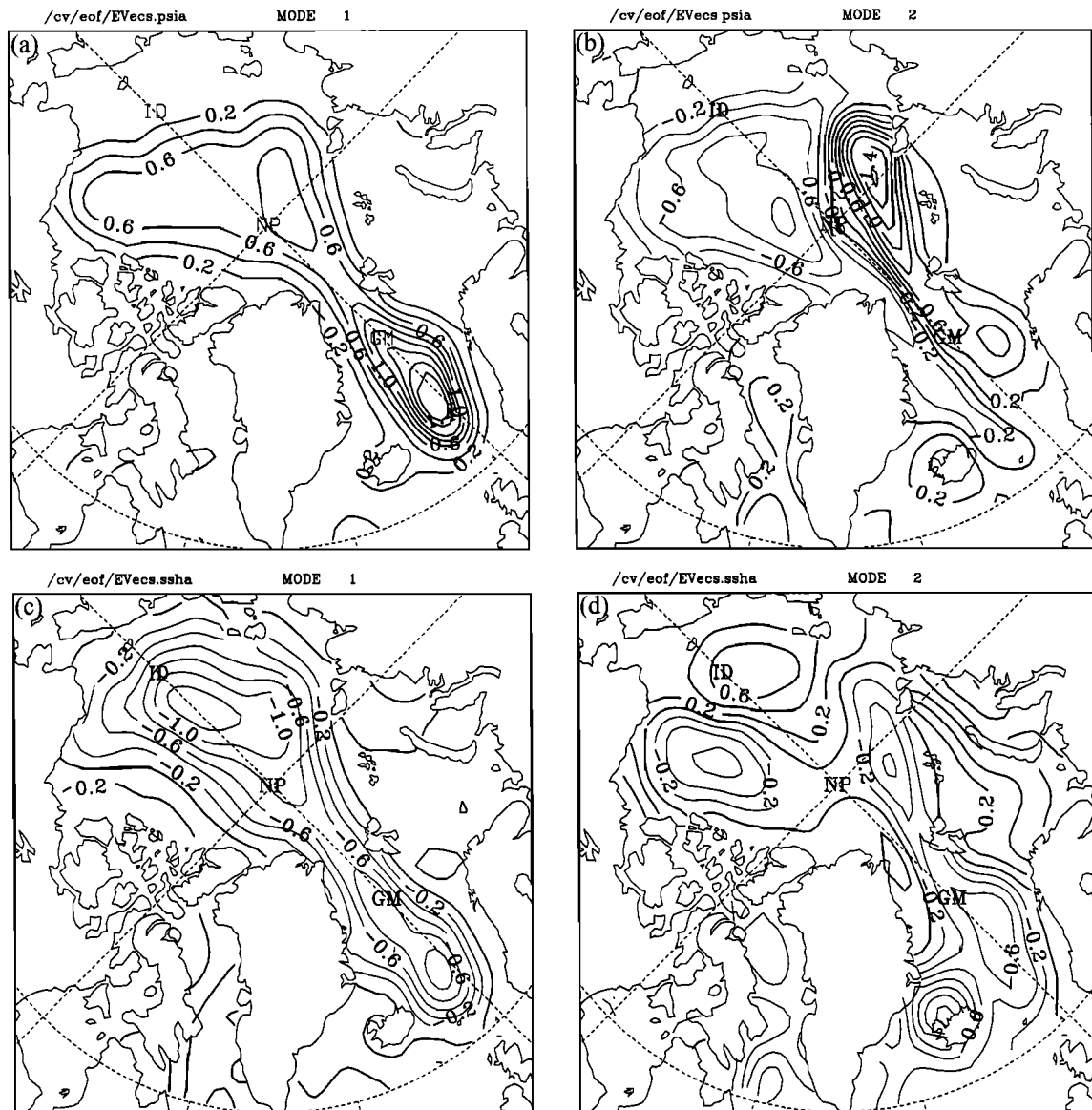


Figure 8. EOF 1 and EOF 2 of (a and b) oceanic stream function and (c and d) SSH. Nondimensional contour interval is 0.2. For stream function, negative values indicate anticyclonic motion, and positive ones indicate cyclonic motion.

the shift may be real. The transport variability inferred from stream function PC 1 of about ± 8 Sv represents a considerable relative change from the mean, as the net transport in the west Spitsbergen Current is ~ 5 Sv (Figure 7a). The PC 2 has much weaker amplitude, ± 2 Sv. Both stream function and SSH show large variations in the recent decades, first toward a strongly anticyclonic regime in the mid-1980s, followed by a shift toward a cyclonic regime after 1988, unprecedented in the simulated record.

Since the time series is only 43 years in length, spectral analysis will have difficulty in assessing decadal periods with significance in the data. To illustrate the frequencies with the most power, we performed a singular spectrum analysis (SSA) [Vautard *et al.*, 1992], which is a data-adaptive method suitable to analyze nonstationary and short time series. SSA of the seasonally binned stream function and SSH PC 1 and PC 2 was performed with a 14.5 year window, which satisfies two requirements for statistical stability: (1) contains at least once the

oscillatory mode of interest and (2) does not exceed one third of the time series. The leading modes appear as pairs of nearly equal eigenvalues well separated from the neighboring eigenvalues (Figures 9c and 9d and 10c and 10d). Using SSA, the mode 1 and 2 basis functions contain cycles with characteristic periods of 9–10 years which explain 12–13% of the variance in stream function PC 1 (Figures 9c and 9e) and 23–27% in SSH PC 1 (Figure 10c). A time series is reconstructed from these basis functions and is shown in Figures 9a and 10a along the original detrended time series and its 11-season (the 3 month seasons are defined as December–February, March–May, etc.) running mean. The reconstruction shows the lack of stationarity of the 9–10 year cycle: While the beginning and end of the time series in both PC 1 show variability at this periodicity, the years 1966–1978, the GSA period, do not. The strongest anticyclonic periods, lasting a few years, are centered at 1961, 1974–1978, and 1986. The cyclonic periods are centered at 1956, 1966–1967, and 1980–1982. These regimes were dis-

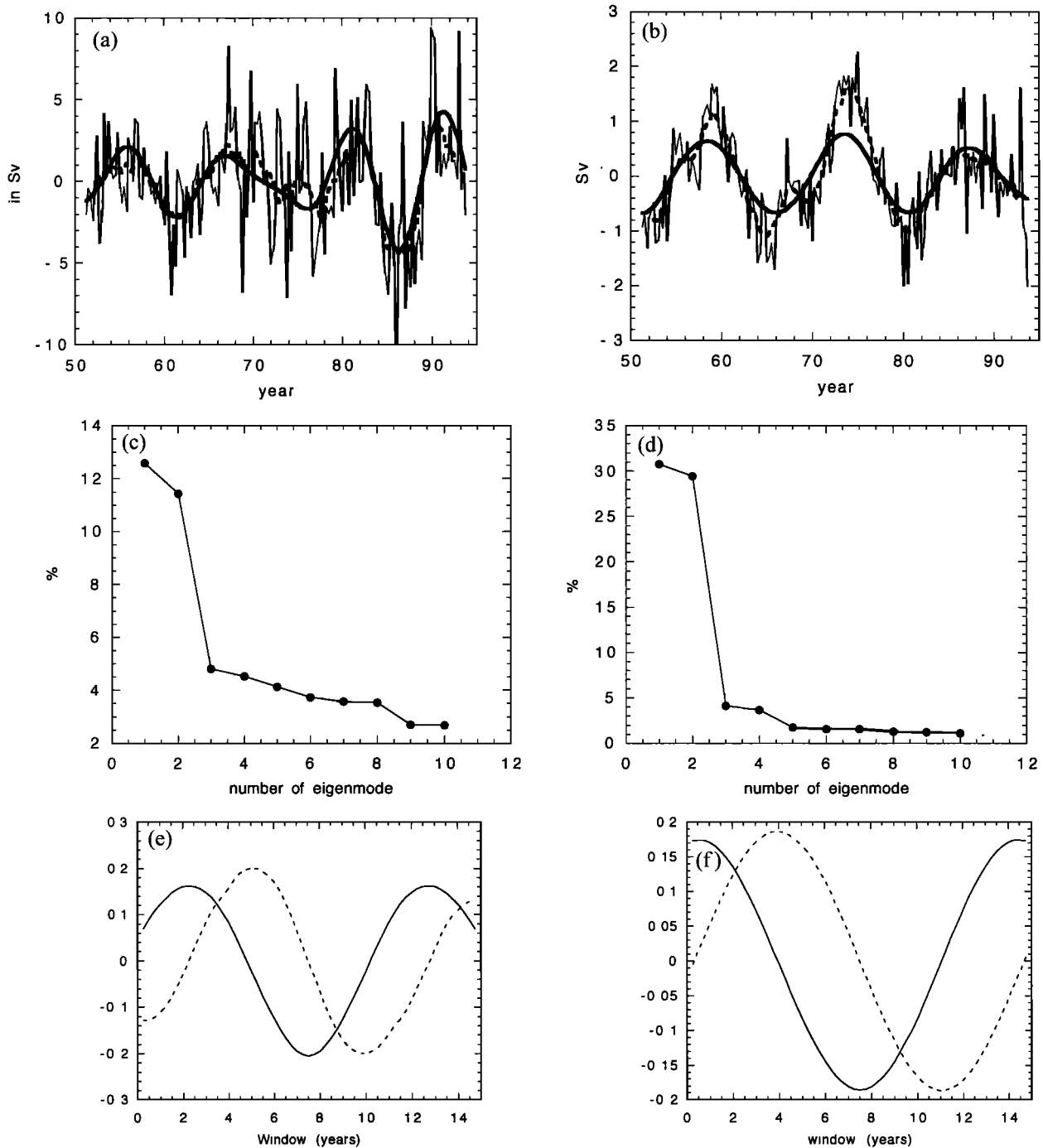


Figure 9. Detrended, seasonally binned oceanic stream function (a) PC 1 and (b) PC 2 (in Sv). Shown also are their low-pass filtered forms (11-point Hanning filter given by dashed line) and the singular spectrum analysis (SSA) reconstruction from the two leading modes (thick solid line). Variances explained by the SSA eigenmodes for (c) PC 1 and (d) PC 2. The SSA eigenmodes 1 and 2 for (e) PC 1 and (f) PC 2.

cussed first by *Proshutinsky and Johnson* [1997]. At the initiation of the GSA period, 1968–1969, the ocean belongs to a weakly cyclonic low-frequency regime (PC 1, Figure 9a), but it has a highly sustained anticyclonic state in 1968–1969 for ~1 year, as indicated by grouping of the negative anomalies through successive seasons. Like PC 1, the PC 2 are characterized by a single strong frequency: Stream function and SSH PC 2 display leading SSA modes with a 14 year cycle have, correspondingly, 29–30% (Figure 11d) and ~10% (Figure

10d) of the variance. The leading SSA modes of SSH PC 2 are not as perfectly regular as the ones of stream function PC 2 (Figure 9f). Their SSA mode 1 and 2 reconstruction and 11-season running mean are shown with seasonally binned time series in Figures 9b and 10b. This quasi-decadal oscillation appears fairly stationary for the last 40 years in the stream function PC 2.

To investigate the source of low-frequency behavior of the stream function PC, we show next that the atmospheric pat-

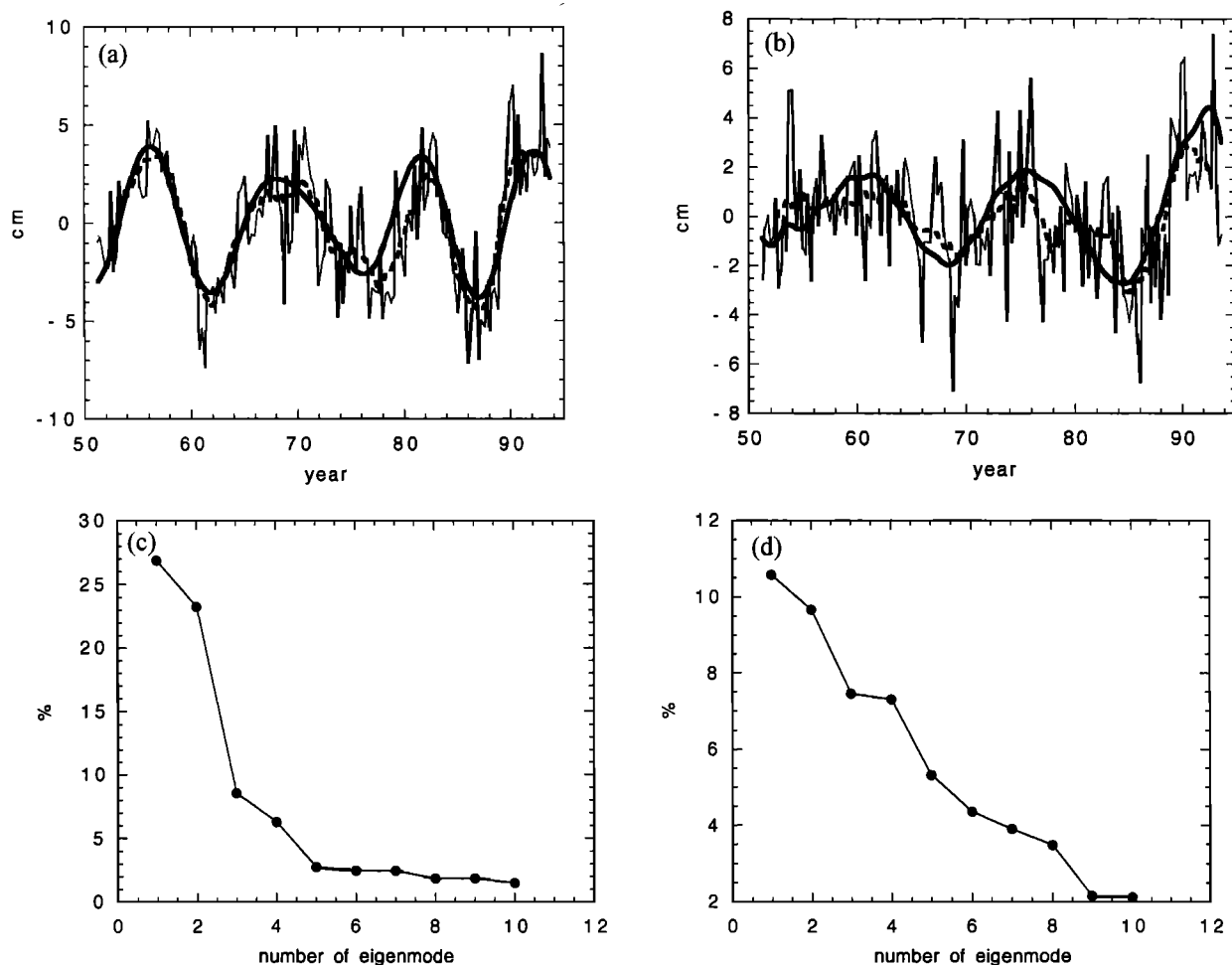


Figure 10. Detrended, seasonally binned sea surface height (a) PC 1 and (b) PC 2 (in cm). Shown also are their low-pass filtered forms (11-point Hanning filter given by dashed line) and the SSA reconstruction from the two leading modes (thick solid line). Variances explained by the SSA eigenmodes for (c) PC 1 and (d) PC 2.

terns composited at their extrema (above one standard deviation; positive minus negative) project on AO- and NAO-like patterns. A SLP composite difference (Figure 11a) at the seasonal extrema of stream function PC 1 when all seasons except summer (June–August) are included into the composite shows a low-pressure system covering the Arctic and the GIN Seas. The pattern in Figure 11a is similar to Figure 1a, which is the Arctic Oscillation (AO) pattern identified by *Thompson and Wallace* [1998]. Correlation between winter (November–April) SLP PC 1 and PC 1 of ocean stream function (and SSH) is 0.52, which is significant at 95% level (using two-tailed t test). Since the SSH and stream function PC 1 are highly correlated at zero lag, which is the only lag with a significant correlation, it is clear that the first mode of oceanic transport is a barotropic response to the AO SLP pattern. The absolute proof of the wind-driven barotropic mode lies in the fact that *Proshutinsky and Johnson* [1997] produced the same variability of the sea level in the central Arctic using a barotropic ocean model. A correlation at zero lag between SLP field and stream function PC 1 results also in a pattern similar to the spatial structure of SLP EOF 1 (not shown). The fact that the first oceanic circulation mode with over 70% of the variance is a barotropic mode is evidence of the dominating one-way coupling between the Arctic atmosphere and ocean (and ice).

There is no reason to expect that barotropic wind-driven motion exhibits low-frequency behavior of its own unless such frequency exists in the SLP field itself. To explore the variability in AO, we use the winter NAO index by *Hurrell* [1995] as a proxy for AO in order to expand the time series to 95 years. SSA with 21 year window is done on the NAO index, and the resulting modes 3 and 4 with near-decadal variability are plotted in Figure 12a along with the variances explained by the first 10 modes (Figure 12b). Eigenmodes 1 and 2 represent quasi-biennial oscillation (2–3 year period) with $\sim 9\%$ of the variance. The third and fourth eigenmodes contain 7% of the variance and can be considered a significant frequency because they are well separated from the neighboring pairs. A similar significant periodicity (7.3 years) using Fourier analysis was retrieved by *Rogers* [1984] for winter NAO. If one uses the winter values of the standardized NAO index (for 1950–1998) by NCEP or the SLP PC 1 (for 1946–1995), the subdecadal mode appears as the third and fourth eigenmodes with ~ 8 year period but is somewhat irregular compared to the one from the longer time series. *Mann and Park* [1996] analyzed joint SST-SLP modes for period 1899–1993 and found a decadal period of 10–11 years where the SLP pattern is similar to NAO pattern. Again, this mode is evident only in winter. Thus winter SLP fields do contain a near-decadal frequency responsible for

the leading oceanic mode. The interesting result is that while the subdecadal period has less power than the quasi-biennial period in the atmosphere, in the ocean the lower frequency has more power. This reversal can be explained by the slow adjustment of the Arctic Ocean: *Galt* [1973] studied the spin-up of a barotropic Arctic Ocean and found it to take a couple of years because of the nearly nonexistent planetary waves. The latter are replaced by topographic Rossby waves, so that the adjustment time is constrained by the slowest (weakest slope) topographic waves. Since the adjustment time is longer than a year, the ocean cannot fully respond to a “high-frequency” variability represented by the quasi-biennial variability.

The second mode of the stream function has a SLP composite difference (Figure 11b) that contains a dominating low in the Denmark Strait and a high near the Azores, resembling a typical NAO (high index phase) SLPA pattern resulting from an EOF analysis for the North Atlantic sector only. Furthermore, no significant correlation for any lags exists between any of the winter (November–April) SLP indices (NAO, SLP PC 1, and SLP PC 2) and stream function PC 2. Even though the stream function PC 2 projects on a NAO-like pattern, NAO is known not to have a 12–14 year periodicity [*Rogers*, 1984], but the 12–14 year period is a prominent timescale of the midlatitude Atlantic surface temperature variability [*Deser and Blackmon*, 1993]. This periodicity is likely to reflect ocean-atmosphere variability in the main North Atlantic, as will be discussed in section 3.4.2. However, this paper is not aiming to resolve the source of the quasi-decadal variability in either domain; we only report that such connection exists. Moreover, the lack of similar significant frequencies in the ocean and atmosphere at quasi-decadal scales is a well-known dilemma of the midlatitude variability.

3.4. Physical Interpretation of the Two Leading Modes

3.4.1. Mode 1: Atlantic water inflow to the Arctic. The time series of the leading oceanic circulation mode shows strong anomalous cyclonic circulation since 1988, with unprecedented monthly variability in the simulated record. The spatial pattern of the first mode of the ocean circulation (Figure 8a) gives an impression that it represents changes in the Atlantic water inflow into the main Arctic basin. To investigate the Atlantic water inflow to the Arctic at Fram Strait, we compute a volume transport for water masses which satisfy a criterion of having temperature warmer than 1°C. This time series is shown in Figure 13. The simulated long-term average inflow is 5–6 Sv, but in the mid-1980s the inflow decreased dramatically to the lowest values. However, since 1989 onward, the inflow has soared to record high values with some monthly values reaching nearly 20 Sv. This event initiated in 1989 can be interpreted as the beginning of the Atlantic layer warming in the Arctic. Wintertime (November–April) correlation between the oceanic stream function PC 1 (positive values denote flow in because the EOF 1 is cyclonic; Figure 8a) and the inflow time series is 0.91 at zero lag. Additionally, correlation between the wintertime inflow and SLP PC 1 (AO) is 0.57 (significant at 95% confidence level), as expected since stream function PC 1 was also well correlated with SLP PC 1. Figure 13 also shows the observed summer temperatures for 50–200 m water column in the West Spitsbergen Current for 1978–1990, adapted from *Loeng et al.* [1992]. The temperatures reflect both the local heat balance and the strength of the currents off Spitsbergen, but in the summertime, heat exchange is limited to the shallow mixed layer waters (<50 m). Thus in-

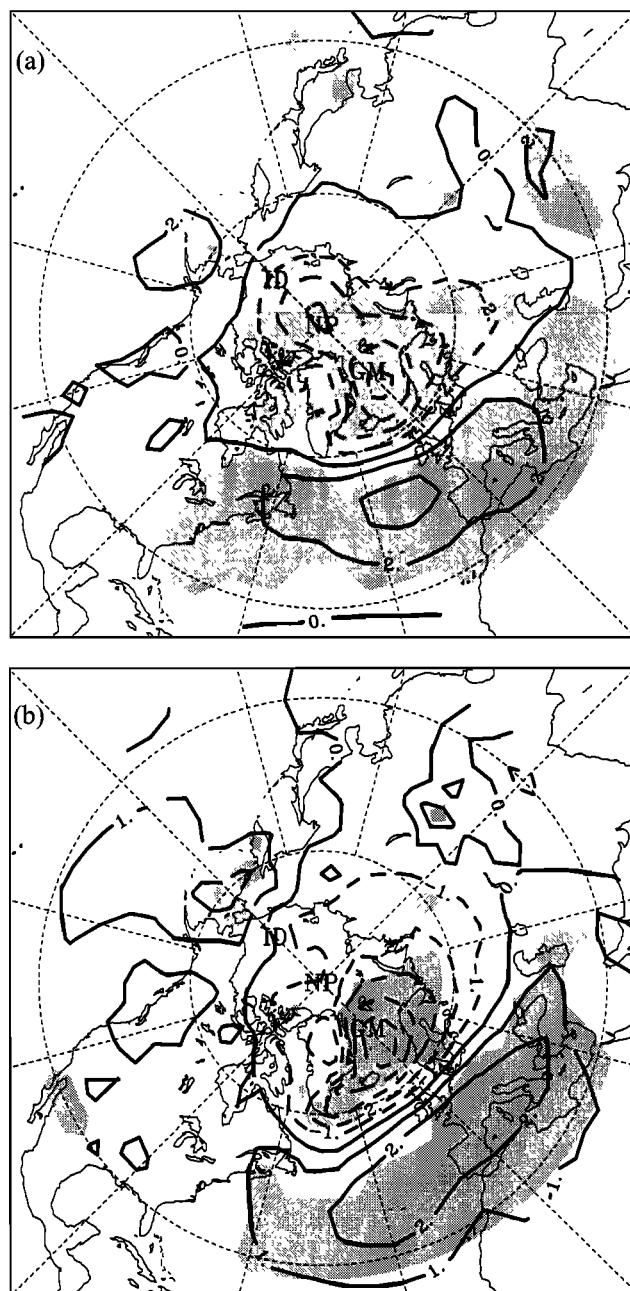


Figure 11. (a) SLP composite difference at the seasonal extrema (summer season (June–August) excluded) of stream function PC 1 (above one standard deviation). Contour interval is 1 hPa. (b) SLP composite at the seasonal extrema (June–August excluded) of stream function PC 2 (above one standard deviation). Contour interval is 1 hPa. Shading indicates that the difference is significant at 95% confidence level.

creasing temperatures at 50–200 m depth should reflect increased advection, which is why we use the observed temperature as a proxy for the transport of the Atlantic water to the Arctic. (The model cannot resolve the high-temperature core of the West Spitsbergen Current; thus no comparison to model temperature is made.) Indeed, the modeled transport and observed temperatures indicate similar variability, although temperature variations are lagging by ~6–12 months the model predicted inflow changes. The similarity between the model transport and the observed temperatures enforces the hypoth-

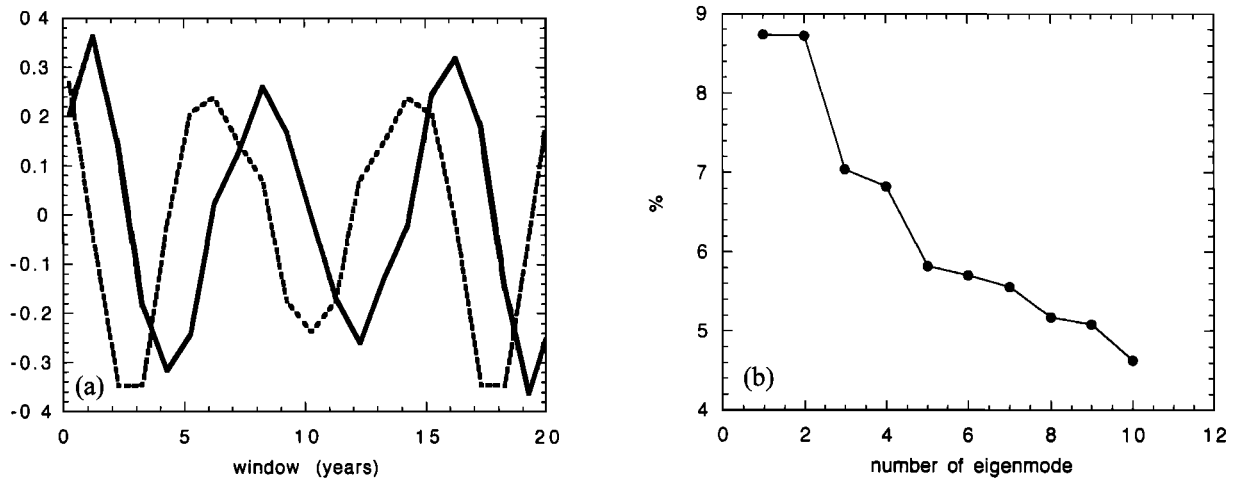


Figure 12. SSA modes for winter NAO index: (a) eigenmodes 3 and 4 containing 8–9 year periodicity and (b) variances explained by the first 10 eigenmodes.

esis that the large changes as measured by AO atmospheric forcing are manifested in the oceanic circulation and specifically in the Atlantic inflow to the Arctic.

Changes in the inflow of the Atlantic water carry changes in the ocean heat content within it. To explore the fate of the heat content changes in the Arctic, we construct composites of the upper 1000 m heat content based on stream function PC 1. It is a more general measure of inflow to the Arctic than the above defined inflow at the Fram Strait based on a temperature criterion. The untrended model data were used to create the composite differences of the heat content at the PC 1 seasonal extrema (above one standard deviation) to highlight the warming event starting in 1989. The sequence of the heat content evolution at lags 0–5 years after the extrema in PC 1 is shown in Figures 14a–14f where heat content field corresponding to negative extrema is subtracted from fields corresponding to positive extrema. When stream function PC 1 is positive, the anomalous flow is strongly cyclonic, i.e., into the Arctic, which is manifested as a positive heat content anomaly along the southern wall of the Eurasia basin where Atlantic water comes in. Consequently, the influence of the increase in Atlantic water heat content spreads cyclonically with the mean flow at the Siberian side of the basins, eventually spreading toward the center in the Canadian and Makarov basins, where it finally dissipates. The heat anomaly loses a considerable amount of its strength off the Laptev Sea, which has been well known to Russian researchers as the sink of the Atlantic water (I. Polyakov, personal communication, 1999). At lag of 5 years (Figure 14f) the pattern shows evidence of a reversal of the pattern at lag 0 (Figure 14a). As noted earlier, the stream function PC 1 has periodicity with ~9–10 years, which also appears here in the timing of the heat content reversal. The heat content cycle shows that the anomalies are mostly locally (to GIN Seas) generated owing to intensification of the barotropic wind-driven circulation. The composites do not indicate movement of the heat content anomalies from south across the Nordic sills (e.g., at lag 0); that is, the increased northward Atlantic water is compensated locally to the GIN Seas (in Figure 8b streamlines are closed, some wrapping around Iceland). Since the mass transport is not replaced from lower latitudes, negative heat content anomalies are initiated (Figures 14a–14c) by intrusion of cold shelf waters to the eastern basin, which ap-

pear much larger when occupying shallow waters around Iceland and in the Barents Sea. The conclusion from the evolution of the heat content changes caused by AO is that since the anomalous heat content is dissipated within the Arctic basin, it does not appear that the anomalies are going to exit the Arctic. Their reemergence within the top 1000 m water column would have provided connection to the global ocean by modifying the overflow at the Nordic Sills. Thus the climatic impact of the heat content anomalies due to AO appear to be confined to the Arctic basin, at least in the ocean component.

3.4.2. Mode 2: Deep water formation in the Barents Sea. The physical interpretation of the second mode of the oceanic transport is not straightforward, but baroclinic processes with the distinct timescale of ~12–14 years exist outside the Arctic: *Deser and Blackmon* [1993] show that such periodicity is present in the leading modes of the North Atlantic surface temperature variability. This timescale is apparent also in the meridional overturning cell of this model at the midlatitudes

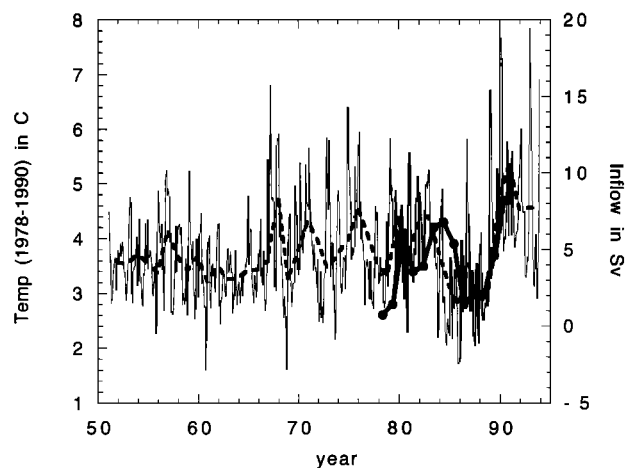


Figure 13. The simulated Atlantic inflow (in Sv, on the right) to the Arctic defined as a net flow with temperature $>1^{\circ}\text{C}$. The thick dashed line is the annual mean value. The thick solid line represents temperatures (in $^{\circ}\text{C}$, on the left) in a 50–200 m layer off Spitsbergen; the temperature values are adapted from *Loeng et al.* [1992].

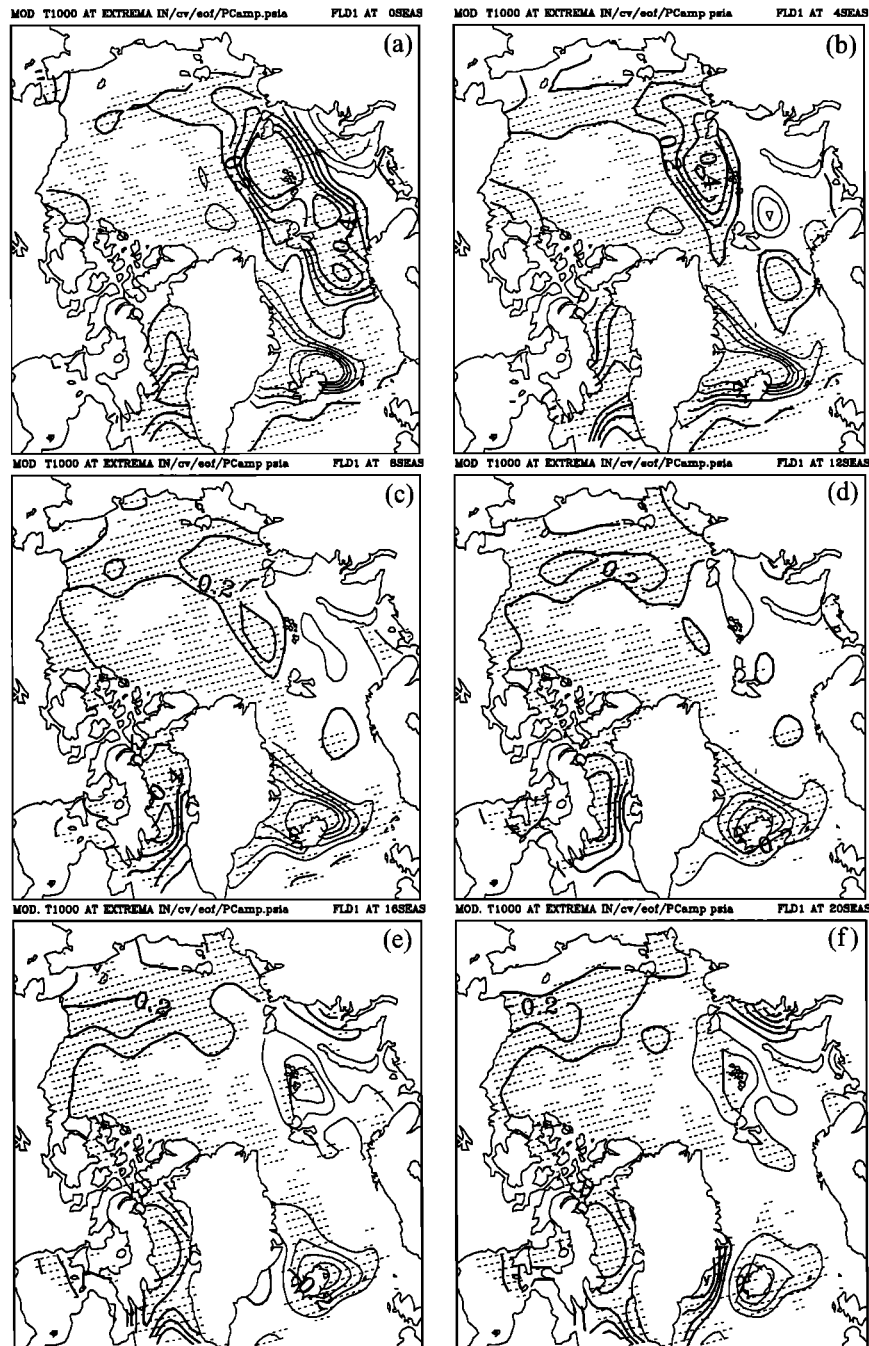


Figure 14. Composite of the upper 1000 m (or the bottom depth, whichever is less) average temperature at the seasonal extrema of stream function PC 1 (above one standard deviation) for lags (a) 0, (b) 4, (c) 8, (d) 12, (e) 16, and (f) 20 seasons. Contour interval is 0.1°C . Hatched areas indicate that the difference is significant at 95% confidence level.

and in the subpolar gyre [Häkkinen, 1999b]. The second mode explains a rather small portion of variance for the stream function (9.2%), but it is of interest, as it should be related to the horizontal transport changes due to overturning and sinking, which are the source of similar variability in the main Atlantic. The sinking motion is compensated by horizontal transport changes reflected in EOF 2/PC 2. The midlatitude example of this concept is the strength of the Gulf Stream: The wind-driven Sverdrup transport is greatly enhanced by the thermohaline circulation (but also by formation of recircula-

tion gyres). The overturning cell in the Arctic is of the order of 6 Sv [Mauritzen and Häkkinen, 1999], thus the PC 2 amplitude of ± 1.5 Sv represents $\pm 25\%$ variability, which is not unreasonable compared to the midlatitude variability.

The investigation of the possible relationship between the Arctic second mode and sinking requires one to find the location of the (anomalous) sinking. The Barents Sea has been considered by many as a major source of deep waters in the Arctic (with additional sources in the Arctic Ocean shelf areas) and would be the first place to consider [e.g., Midttun, 1989].

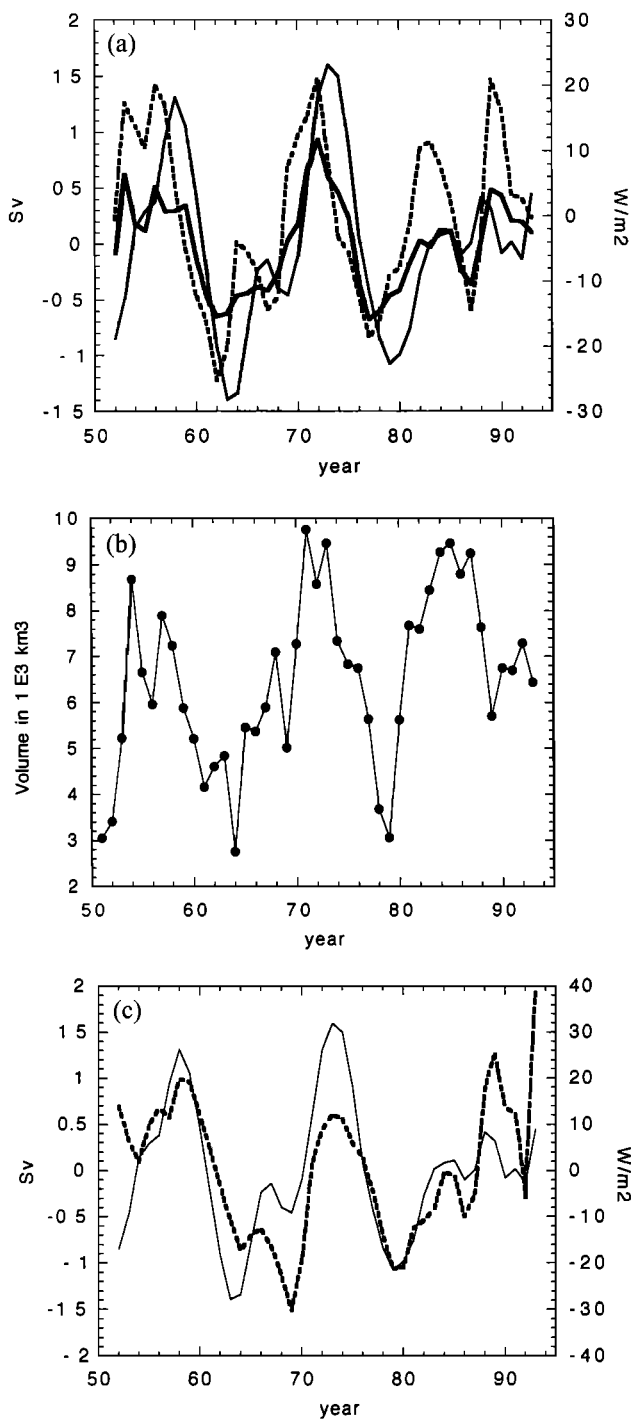


Figure 15. (a) The Barents Sea through flow (thick solid line) and the stream function PC 1 (thin solid line) (both in Sv, with scale on the left) and Barents Sea heat flux (dashed line; positive values denote heat loss) (in W/m^2 , scale on the right). (b) The annual cumulative volume (in km^3) of waters heavier than $28.0 \sigma_0$ units in the Barents and Kara Seas. (c) Stream function PC 2 (solid line, scale on the left) and the time series of the leading North Atlantic heat flux mode (dashed line, scale on the right). All values are November to April averages.

The large heat flux in the Barents Sea, occupied by Atlantic origin waters, provides the process to form the deep waters which flow off to the Eurasia basin. If the water mass residence time in the Barents Sea is the order of a cooling season,

enhanced sinking due to heat loss increase must be compensated by a change in inflow. To demonstrate this simple relation, the anomalous heat flux (heat loss from the ocean is positive) in the Barents Sea and the anomalous through flow to the Barents Sea are depicted in Figure 15a; the values are November through April averages smoothed once by one binomial filter. (The section where the through flow is computed is shown in Figure 8b.) There is a remarkable simultaneous correlation between the two quantities, which supports the simple explanation of sinking driven by heat flux variations. The stream function PC 2 is also plotted in Figure 15a, which shows similar behavior with ~ 1 year lag. As a note, there are no significant correlations between the Barents Sea through flow and stream function PC 1, which also supports the notion that PC 2 is determined by other processes than wind driving. To show that the waters forming in the Barents-Kara Seas are indeed deep waters, or at least contribute to the heaviest part of the Atlantic layer, the annual cumulative sum of water masses heavier than $28.0 \sigma_0$ units is plotted in Figure 15b. It follows closely the envelope of heat flux anomalies. It is noteworthy that in comparison with the through flow, during the 1980s the cumulation was high, but the through flow anomaly, as well as PC 2, was small. This time period experienced extremely strong anticyclonic anomaly in the barotropic component of the circulation (Figure 9a), which should prevent the outflow from the Barents shelf leading to accumulation of heavy waters on the shelves. Figure 15a is in agreement with this scenario: Since the sinking was prohibited, the through flow and PC 2 remained small.

To explore the connection of PC 2 to NAO (composite in Figure 11b), we had to involve the main North Atlantic heat flux, discussed in detail by Häkkinen [1999b]. The NAO connection emerges because PC 2 varies in phase with the leading mode of heat flux in the midlatitude North Atlantic (simultaneous correlation of 0.52 between the November–April average values) (Figure 15c) which is associated with variability in NAO. These two factors together suggest that the maximum Barents Sea heat loss precedes, by ~ 1 year, the maximum heat flux associated with NAO. Even though it is an intriguing connection, it is unlikely that the small transport changes into the Barents Sea have much influence on the midlatitude atmosphere-ocean processes.

4. Summary

Variability of sea ice cover from a 43 year coupled ice-ocean model simulation for the period 1951–1993 is analyzed to determine causal mechanisms. The ice motion was investigated using composites based on the leading hemispheric SLP mode, for which *Thompson and Wallace* [1998] has suggested the name of Arctic Oscillation. As the sea ice motion adjusts within a day to the overlaying wind stress field, the resulting ice motion anomalies reflects basically the anomalous geostrophic wind field, which produces two seesaw patterns: one between Beaufort Sea–Canadian Archipelago and East Siberian–Laptev Seas and one between Kara-Barents (GIN) Seas and Baffin Bay. Our simulation shows that AO does not have much influence on the sea ice export through Fram Strait; instead, the SLPA pattern responsible for increased ice export resembles the negative NAO index SLP pattern with a high over Greenland and a low over Azores. Concerning the ice export through Denmark Strait to the subpolar gyre, *Mauritzen and Häkkinen* [1997] and *Häkkinen* [1999a] conclude that the Denmark Strait

export has a more significant role in modulating overturning in the North Atlantic than the Fram Strait export. The latter is the source for the excess ice, but for an oceanic overturning response, either excess ice export through both straits has to be maintained for several years, or it has to be a one time event where the excess ice exits Denmark Strait in an intense pulse. The Denmark Strait export is controlled by a local SLPA pattern consisting of an intense low east of Iceland, thereby giving rise to strong northeasterly winds. The influence of the local atmospheric conditions without a significant hemispheric signal has also been found to control the sea ice conditions around Iceland, as recorded by the Icelandic Ice Index [Kelly *et al.*, 1987].

The sea surface height and oceanic transport stream function are studied using EOF to find the most prominent modes of variability. As one would expect, their first modes are similar where the whole basin operates in unison as a single gyre, and in fact, the two PC are highly correlated at zero lag. The first and second modes of the oceanic stream function explain 71 and 9% of the total variance. The second mode of the oceanic stream function contains two gyres, one in the Canada Basin and the other in the Eurasia-GIN Seas basin, which have an opposite sense of rotation. The time series associated with the first mode contains large variations, and one such fluctuation since 1989 is toward a strong cyclonic circulation unprecedented in the simulated time series. The first mode of the oceanic stream function can be associated with the inflow variations of the Atlantic waters entering through Fram Strait; these two quantities can explain over 80% of each other's variance (wintertime). We anticipate that the shift toward more cyclonic circulation in 1989 initiated the warming of the Atlantic layer in the Arctic. The associated heat content changes will circulate cyclonically in the Arctic basin with the mean flow and dissipating after a few years in the Canada Basin. In this simulation the heat content anomalies do not reemerge outside the Arctic in order to influence the Nordic Sills overflow waters.

We find that the primary oceanic circulation mode in the Arctic is associated with the Arctic Oscillation pressure pattern where the atmosphere is driving the ocean (and ice). Specifically, the shift toward a strong cyclonic circulation anomaly after 1989 can be related to the intensification of the AO. Both a significant correlation between SLP and stream function PC 1 and the SLP composite at the extrema of stream function PC 1 confirm this barotropic response of the ocean. Using SLP composites, the second mode of the oceanic stream function projects onto a atmospheric pattern resembling NAO, although its PC 2 is not correlated with NAO index. If there is a causal connection between the PC 2 and NAO, it has to be an indirect one. In fact, we find this NAO connection to arise because PC 2 is significantly correlated with the leading heat flux mode from the midlatitude North Atlantic. This North Atlantic heat flux mode is associated with NAO [Häkkinen, 1999b]. More importantly, this second Arctic mode follows with ~ 1 year lag the variability of the deep water formation in the Barents Sea. The latter quantity is shown to be associated to the net inflow variability to the Barents Sea, which together with local heat flux, conforms to a hypothesis of the water mass formation and exits from the area.

Using singular spectrum analysis [Vautard *et al.*, 1992], we find that the oceanic stream function displays subdecadal variability at ~ 9 year and at 12–14 year periodicity. These two frequencies are divided between the leading modes such that the shorter (9 years) fluctuations are in the first mode, and the

longer period, 12–14 years, variations are in the second mode of ocean circulation. Observations also suggest the existence of two slightly different decadal frequencies: Wintertime NAO index has a peak at ~ 8 years [Rogers, 1984], and Labrador tree ring density chronologies and ice cores indicate statistically significant spectral peaks for 8.7 years [D'Arrigo *et al.*, 1996; Barlow *et al.*, 1993], while the 12–14 year period is a known periodicity in the subpolar-subtropical gyres [Deser and Blackmon, 1993]. We presented evidence that the dominant decadal period, ~ 9 years, in the high-latitude ocean is produced by local (wintertime) wind forcing. The source of this subdecadal prominent periodicity in the atmosphere is not known, but it could result either from ocean-atmosphere coupling or from intrinsic atmospheric variability. The 12–14 year periodicity in the oceanic transport can only be interpreted as the lower latitude influence on the Arctic ocean circulation.

In summary, on the basis of the presented analysis it is unlikely that the Arctic atmosphere-ocean-ice system would behave as a closed entity to give rise to a self-contained coupled mode at either of these two frequencies. A differing view can be found from a recent study by Mysak and Venegas [1998] who suggest coupling, but the evidence here and the results of Proshutinsky and Johnson [1997] (using a barotropic ocean model), Walsh and Sater [1981], and Fang and Wallace [1994] support one-way coupling of atmosphere driving the ice-ocean system. Although only a stand-alone ice-ocean model was used here, its atmospheric forcing contains all possible interactions in the atmosphere-ice-ocean system, local and nonlocal, simultaneous and delayed. Even in this framework, a simple diagnostic of positive feedback between ocean/ice and atmospheric quantities, a requirement for a two-way coupling, can be tested: It amounts to finding statistically significant correlations between ocean/ice and atmospheric quantities when the ocean/ice quantity leads at timescales from weeks to a year or two, while the maximum correlation (with the same sign as for ocean/ice leading) would still be found either simultaneously or when the atmosphere leads. No such correlations were found, as was the case in the studies of Walsh and Sater [1981] and Fang and Wallace [1994]: Walsh and Sater [1981] showed consistently higher correlations with atmospheric indices leading (or simultaneous with) the ice indices and lack of correlations if ice leads; Fang and Wallace [1994] showed that the strongest relationship between SLP variations and sea ice concentration changes occur when SLP leads by 2 weeks. Undoubtedly, modeling experiments using fully coupled models will clarify the issue of local coupling at high latitudes, but high expectations on coupled model results may be unwarranted. This is because even if one would find a scenario of plausible physical processes (in addition to albedo feedback) that could mediate the coupling, it is another matter whether the resulting signal carries any significance compared to the large internal atmospheric variability. Whether coupled processes exist between the combined Arctic-Atlantic system is a more relevant question for a coupled models.

Acknowledgments. This work was supported by NASA Headquarters Polar Programs. Programming support was provided by Lena Marshak.

References

- Agnew, T., Simultaneous winter sea-ice and atmospheric circulation anomaly patterns, *Atmos. Ocean*, 31, 259–280, 1993.
- Barlow, L. K., J. W. C. White, R. G. Barry, J. C. Rogers, and P. M. Grootes, The North Atlantic Oscillation Signature in deuterium and

- deuterium excess signals in the Greenland Ice Sheet Project 2 Ice cores, 1840–1970, *Geophys. Res. Lett.*, *20*, 2901–2904, 1993.
- Barnston, A. G., and R. E. Livezey, Classification, seasonality, and persistence of low-frequency atmospheric circulation patterns, *Mon. Weather Rev.*, *115*, 1083–1126, 1987.
- Blumberg, A. F., and G. L. Mellor, A description of a three-dimensional coastal ocean circulation model, in *Three-Dimensional Coastal Ocean Models*, *Coastal Estuarine Sci.*, vol. 4, edited by N. S. Heaps, pp. 1–16, AGU, Washington, D. C., 1987.
- Carmack, E. C., R. W. Macdonald, R. G. Perkin, F. A. McLaughlin, and R. J. Pearson, Evidence of warming of Atlantic water in the southern Canadian Basin of the Arctic Ocean, *Geophys. Res. Lett.*, *22*, 1061–1064, 1995.
- Cavaliere, D. J., P. Gloersen, C. L. Parkinson, J. C. Comiso, and H. J. Zwally, Observed hemispheric asymmetry in global sea ice changes, *Science*, *278*, 1104–1106, 1997.
- Cheng, X., G. Nitsche, and J. M. Wallace, Robustness of low-frequency circulation patterns derived from EOF and rotated EOF analyses, *J. Clim.*, *8*, 1709–1713, 1995.
- D'Arrigo, R. D., E. R. Cook, and G. C. Jacoby, Annual to decadal-scale variations in northwest Atlantic sector temperatures inferred from Labrador tree rings, *Can. J. For. Res.*, *26*, 143–148, 1996.
- daSilva, A. M., C. C. Young, S. Levitus, *Atlas of Surface Marine Data 1994*, vol. 1, *Algorithms and Procedures*, NOAA Atlas Ser., Natl. Oceanic and Atmos. Admin., Silver Spring, Md., 1994.
- Deser, C., and M. L. Blackmon, Surface climate variations over the North Atlantic Ocean during winter: 1900–1989, *J. Clim.*, *6*, 1743–1753, 1993.
- Dickson, R. R., J. Meincke, S.-A. Malmberg, and A. J. Lee, The “Great Salinity Anomaly” in the northern North Atlantic 1968–1982, *Prog. Oceanogr.*, *20*, 103–151, 1988.
- Fang, Z., and J. M. Wallace, Arctic sea ice variability on a timescale of weeks and its relation to atmospheric forcing, *J. Clim.*, *7*, 1897–1914, 1994.
- Galt, J. A., A numerical investigation of Arctic Ocean dynamics, *J. Phys. Oceanogr.*, *3*, 379–396, 1973.
- Häkkinen, S., An arctic source for the Great Salinity Anomaly: A simulation of the Arctic ice ocean system for 1955–1975, *J. Geophys. Res.*, *98*, 16,397–16,410, 1993.
- Häkkinen, S., Simulated interannual variability of the Greenland Sea deep water mass formation and its connection to surface forcing, *J. Geophys. Res.*, *100*, 4761–4770, 1995.
- Häkkinen, S., A simulation of thermohaline effects of a Great Salinity Anomaly, *J. Clim.*, *12*, 1781–1795, 1999a.
- Häkkinen, S., Variability of the simulated meridional heat transport in the North Atlantic for the period 1951–1993, *J. Geophys. Res.*, *104*, 10,991–11,007, 1999b.
- Häkkinen, S., and G. L. Mellor, Modeling the seasonal variability of the coupled Arctic ice-ocean system, *J. Geophys. Res.*, *97*, 20,285–20,304, 1992.
- Halliwel, G. R., and D. A. Mayer, Frequency response properties of forced climatic SST anomaly variability in the North Atlantic, *J. Clim.*, 3575–3587, 1996.
- Hilmer, M., M. Harder, and P. Lemke, Sea ice transport: A highly variable link between Arctic and North Atlantic, *Geophys. Res. Lett.*, *25*, 3359–3362, 1998.
- Hurrell, J. W., Decadal trends in the North Atlantic Oscillation regional temperatures and precipitation, *Science*, *269*, 676–679, 1995.
- Kelly, P. M., C. M. Goodess, and B. S. G. Cherry, The interpretation of the Icelandic sea ice record, *J. Geophys. Res.*, *92*, 10,835–10,843, 1987.
- Levitus, S., and T. P. Boyer, *World Ocean Atlas 1994*, vol. 4, *Temperature*, NOAA Atlas NESDIS 4, Natl. Oceanic and Atmos. Admin., Silver Spring, Md., 1994.
- Levitus, S., R. Burgett, and T. P. Boyer, *World Ocean Atlas 1994*, vol. 3, *Salinity*, NOAA Atlas NESDIS 3, Natl. Oceanic and Atmos. Admin., Silver Spring, Md., 1994.
- Loeng, H., J. Blindheim, B. Adlandsvik, and G. Ottersen, Climatic variability in the Norwegian and Barents Seas, *ICES Mar. Sci. Symp.*, *195*, 52–61, 1992.
- Mann, M. E., and J. Park, Joint spatiotemporal modes of surface temperature and sea level pressure variability in the Northern Hemisphere during the last century, *J. Clim.*, *9*, 2137–2162, 1996.
- Mauritzen, C., and S. Häkkinen, Sensitivity of thermohaline circulation to sea-ice forcing in an Arctic-North Atlantic Model, *Geophys. Res. Lett.*, *24*, 3257–3260, 1997.
- Mauritzen, C., and S. Häkkinen, On the relationship between dense water formation and the “Meridional Overturning Cell” in the North Atlantic Ocean, *Deep Sea Res., Part I*, *46*, 877–894, 1999.
- McLaughlin, F. A., E. C. Carmack, R. W. Macdonald, and J. K. B. Bishop, Physical and geochemical properties across the Atlantic/Pacific water mass front in the southern Canadian Basin, *J. Geophys. Res.*, *101*, 1183–1197, 1996.
- Mellor, G. L., and L. H. Kantha, An ice-ocean coupled model, *J. Geophys. Res.*, *94*, 10,937–10,954, 1989.
- Mellor, G. L., and T. Yamada, Development of a turbulence closure model for geophysical fluid problems, *Rev. Geophys.*, *20*, 851–875, 1982.
- Midttun, L., Climatic fluctuations in the Barents Sea, *Rapp. P. V. Reun. Cons. Int. Explor. Mer.*, *188*, 23–35, 1989.
- Mysak, L. A., and S. A. Venegas, Decadal climate oscillations in the Arctic: A new feedback loop for the atmosphere-ice-ocean interactions, *Geophys. Res. Lett.*, *25*, 3607–3610, 1998.
- Parkinson, C. L., D. J. Cavaliere, P. Gloersen, H. J. Zwally, and J. C. Comiso, Arctic sea ice extents, areas, and trends, 1978–1996, *J. Geophys. Res.*, *104*, 20,837–20,856, 1999.
- Pocklington, R., Arctic rivers and their discharges, in *SCOPE/UNEP Sonderband, Heft 64*, pp. 261–268, Hamburg, Germany, 1987.
- Proshutinsky, A. Y., and M. A. Johnson, Two circulation regimes of the wind-driven Arctic Ocean, *J. Geophys. Res.*, *102*, 12,493–12,514, 1997.
- Rasmusson, E. M., and K. Mo, Large scale atmospheric moisture cycling as evaluated from NMC global analysis and forecast products, *J. Clim.*, *9*, 3276–3297, 1996.
- Rogers, J. C., The association between the North Atlantic Oscillation and the Southern Oscillation in the Northern Hemisphere, *Mon. Weather Rev.*, *112*, 1999–2015, 1984.
- Rogers, J. C., North Atlantic storm track variability and its association with the North Atlantic Oscillation and climate variability of northern Europe, *J. Clim.*, *10*, 1635–1647, 1997.
- Russell, G. L., and J. R. Miller, Global river runoff calculated from a global atmospheric general circulation model, *J. Hydrol. Amsterdam*, *117*, 241–254, 1990.
- Serreze, M. C., J. E. Box, R. G. Barry, and J. E. Walsh, Characteristics of Arctic synoptic activity, 1952–1989, *Meteorol. Atmos. Phys.*, *51*, 147–164, 1993.
- Serreze, M. C., J. A. Maslanik, J. R. Key, and R. F. Kokaly, Diagnosis of the record minimum in Arctic sea ice area during 1990 and associated snow cover extremes, *Geophys. Res. Lett.*, *22*, 2183–2186, 1995.
- Serreze, M. C., J. C. Rogers, F. Carsey, and R. G. Barry, Icelandic low cyclone activity: Climatological features, linkages with the NAO and relationships with recent climate changes in the Northern Hemisphere circulation, *J. Clim.*, *10*, 453–464, 1997.
- Thompson, D. W. J., and J. M. Wallace, Observed linkages between Eurasian surface air temperature, the North Atlantic Oscillation, Arctic Sea-level pressure and the stratospheric polar vortex, *Geophys. Res. Lett.*, *25*, 1297–1300, 1998.
- Trenberth, K., J. G. Olson, and W. G. Large, A global ocean wind stress climatology based on ECMWF analyses, *NCAR Tech. Note NCAR/TN-338+STR*, 93 pp., Natl. Cent. for Atmos. Res., Boulder, Colo., 1989.
- van Loon, H., and J. C. Rogers, The Seesaw in winter temperatures between Greenland and northern Europe, part I, General description, *Mon. Weather Rev.*, *106*, 296–310, 1978.
- Vautard R., P. Yiou, and M. Ghil, Singular spectrum analysis: A toolkit for short, noisy chaotic signals, *Physica D*, *58*, 95–126, 1992.
- Walsh, J. E., and J. E. Sater, Monthly and seasonal variability in the ocean-ice-atmosphere systems of the North Pacific and the North Atlantic, *J. Geophys. Res.*, *86*, 7425–7446, 1981.
- Walsh, J. E., W. D. Hibler, and B. Ross, Numerical simulation of Northern Hemisphere sea ice variability, 1951–1980, *J. Geophys. Res.*, *90*, 4847–4865, 1985.
- Walsh, J. E., W. L. Chapman, and T. Shy, Recent decrease of sea level pressure in the central Arctic, *J. Clim.*, *9*, 480–486, 1996.
- C. A. Geiger, University of Delaware, Department of Geography, 216 Pearson Hall, Newark, DE 19716.
S. Häkkinen, NASA Goddard Space Flight Center, Code 971, Greenbelt, MD 20771. (hakkinen@gssc.nasa.gov)

(Received November 9, 1998; revised December 7, 1999; accepted December 29, 1999.)